JGR Space Physics

RESEARCH ARTICLE
10.1029/2019JA027601

Interhemispheric Asymmetry of Large-Scale Electron Density Gradients in the Polar Cap Ionosphere: UT and Seasonal Variations

Yaqi Jin[1] and **Chao Xiong**[2]

[1]Department of Physics, University of Oslo, Oslo, Norway, [2]Helmholtz Centre Potsdam, GFZ German Research Centre for Geosciences, Potsdam, Germany

Key Points:
- Density gradients (100 km) in the Arctic are enhanced from autumn to spring equinoxes with a significant "hole" during 3–12 UT near December solstice
- The variations of density gradients are mirror symmetric for two hemispheres during local winter
- Density gradients in the Antarctic are strong and persistent during local summer (December solstice)

Supporting Information:
- Supporting Information S1

Correspondence to:
Y. Jin,
yaqi.jin@fys.uio.no

Citation:
Jin, Y., & Xiong, C. (2020). Interhemispheric asymmetry of large-scale electron density gradients in the polar cap ionosphere: UT and seasonal variations. *Journal of Geophysical Research: Space Physics*, *125*, e2019JA027601. https://doi.org/10.1029/2019JA027601

Received 6 NOV 2019
Accepted 16 JAN 2020
Accepted article online 3 FEB 2020

Abstract The high-latitude ionosphere is highly dynamical with significant irregularities and density gradients. However, the spatial and temporal distributions of density gradients and irregularities are very different between the Arctic and Antarctic. In this report, we study the interhemispheric asymmetry of the large-scale (100 km) density gradients in both polar caps. Our results show that density gradients in the Arctic are enhanced during local winter (December solstice) with a peak around 19 UT. The UT and spatial distributions in the Antarctic local winter (June solstice) are similar to the Arctic except that they are reversed by 12 hr, which indicates a mirror symmetry between hemispheres. The 12-hr difference in the peak density gradients can be explained by the displacements between the geographic and geomagnetic poles. The only asymmetry (anomaly) is the persistence of strong density gradients in the southern polar cap during local summer (December solstice).

Plain Language Summary The high-latitude ionosphere is highly variable with significant fluctuations in plasma density. So far, the long-term studies have been conducted in the Arctic due to better ground-based data coverage, while the knowledge of the Antarctic is limited. We take advantage of the Swarm mission to study the long-term behaviors in both the Arctic and Antarctic. New statistics reveal phenomena that we understand and an "anomaly" that do not understand. The results during local winter (December in the Arctic and June in the Antarctic) are similar and can be explained by the previous knowledge. However, the anomaly is the persistence of strong density fluctuations in the Antarctic during local summer (December solstice).

1. Introduction

Ionospheric irregularities can be especially detrimental to satellite-based communication and positioning systems that use trans-ionospheric radio signals (Kintner et al., 2007). Steep electron density gradients are very effective sources for generating irregularities; that is, the gradient-drift instability can produce structures on the top of steep density gradients in a time scale of less than a minute (e.g., Moen et al., 2012; Spicher et al., 2015). Therefore, it is important to study the electron density gradient in a general sense. At high latitudes (especially in the polar caps), polar cap patches are the most important bodies for providing large-scale density gradients (e.g., Basu et al., 1991; Carlson, 2012; Jin et al., 2014). Polar cap patches are islands of high-density *F* region plasma with densities 2–10 times higher than the background density. Their spatial scale ranges from 100 to 1,000 km (Crowley et al., 2000).

It is well accepted that the main source of polar cap patches is the photoionization due to solar extreme ultraviolet (EUV) radiation (Carlson, 2012; Tsunoda, 1988). The dayside reconnection-driven convection could bring the sunlit, high-density plasma from lower latitudes to the cusp, and thereafter they are transported into the polar cap (e.g., Anderson et al., 1988; Lockwood & Carlson, 1992). Polar cap patches can move across the polar cap to the nightside open/closed field line boundary, and there they can exit the polar cap during tail reconnection (Jin et al., 2014; Lorentzen et al., 2004; Moen et al., 2007).

Polar cap patches have been studied using ground-based measurements such as ionosondes, all-sky imagers, coherent and incoherent scatter radars, and global positioning system (GPS) receivers (Buchau et al., 1985; Buchau et al., 1988; Carlson et al., 2006; Hosokawa et al., 2009; Rodger & Graham, 1996; Weber et al., 1986). However, most of these studies have been conducted using data from the Arctic. Due to the sparsity of

instruments, it is challenging to study polar cap patches and density gradients in the Antarctic, especially to obtain the long-term statistics. Polar orbiting satellites, such as the Swarm mission, provide an unprecedented opportunity to study electron density gradients in both hemispheres with good spatial coverages.

Due to the asymmetry of the Earth's magnetic field, the near-Earth space environment is asymmetric (e.g., Laundal et al., 2017). This asymmetry and others can lead to an asymmetric distribution of electron density gradients and irregularities between hemispheres. In this study, we investigate the interhemispheric asymmetry of the large-scale density gradient in the polar caps for the first time, and we focus on the seasonal and universal time (UT) variations.

2. Data and Methodology

In this study, we make use of the European Space Agency's Swarm mission. The in situ electron density data from the Langmuir probe are used, which are measured at a rate of 2 Hz (Knudsen et al., 2017; Lomidze et al., 2018).

With the raw electron density, we derive the large-scale density gradient (∇Ne) by using a linear regression over 27 data points (~100 km for Swarm; Jin et al., 2019). We have also tested electron density gradients over different scales (e.g., 50 and 20 km), and the seasonal and UT patterns do not change significantly. We therefore use density gradients over 100 km as a parameter for ionospheric structures in the polar caps.

We exemplify the calculation of density gradients in Figure 1. Figure 1a displays the ground-based GPS total electron content (TEC) map at 18:22 UT on 21 December 2014 in magnetic latitude/magnetic local time (MLAT/MLT) coordinates. The TEC data, in bins of $1° \times 1°$ in geographic latitude and longitude with time resolution of 5 min, are obtained from the Madrigal database (Rideout & Coster, 2006). The TEC map is presented in Magnetic Apex Coordinates (Emmert et al., 2010; Richmond, 1995). The Feldstein auroral oval is overlaid as solid magenta curves to give a guidance of auroral and polar cap areas (Holzworth & Meng, 1975). The input parameter Q of the Feldstein oval is set to 3. The GPS TEC map shows a train of polar cap patches/tongue of ionization in the polar cap. Swarm A flies from postmidnight toward postnoon across the polar cap. Figure 1b shows the raw electron density data in black. Several polar cap patches are observed from the in situ electron density measurement, which is consistent with the TEC map in Figure 1a. We derive three steep density gradients near the edges of polar cap patches at a spatial scale of 100 km. The three steep density gradients are annotated by red dashed lines, which are linear regressions centered at the red dots. Figure 1c shows the density gradients over the running window during the period of interest. Note that the density gradients show positive and negative values when Swarm flies toward and away from a high-density structure. To eliminate this effect, we use absolute values when deriving the statistics in the following sections.

Figures 1d–1f show an example in the southern hemisphere. Figure 1d displays the TEC map, which shows that a train of polar cap patches/tongue of ionization are formed inside the polar cap. Due to the sparsity of GPS observations in the Antarctic, the feature of polar cap patches from the TEC map is not as clear as in the Arctic. However, with the in situ measurement of Swarm satellite, we have continuous observations along the satellite orbit in the Antarctic. This is the main advantage of Low Earth Orbit (LEO) satellites in studying the interhemispheric asymmetry of the ionosphere. Swarm A flies from postnoon to postmidnight. Figure 1e shows that Swarm A observes several polar cap patches with steep density gradients. Figure 1f shows the density gradients over 100 km. Several steep density gradients are observed during the time period of interest.

In the next sections, we will present and discuss the statistics of electron density gradients by using long-term observations of the Swarm spacecraft. Swarm satellites were launched on in November 2013 at about 500-km altitude. Between January and April 2014, Swarm B was raised to around 520-km altitude, while Swarm A and C flew side by side at an altitude of about 480 km. We use data when Swarm flew in the final orbit. The date period is from April 2014 to April 2019, that is, five years of data. During these five years, the orbit altitude dropped from 480 to 450 km. In this study, we only show the statistics from Swarm A, as the results from the other two satellites have similar patterns. The results from Swarm B can be found in the supporting information. The similarity in the statistics from Swarm A and B suggests that our results are not affected by the orbit precession of Swarm satellites.

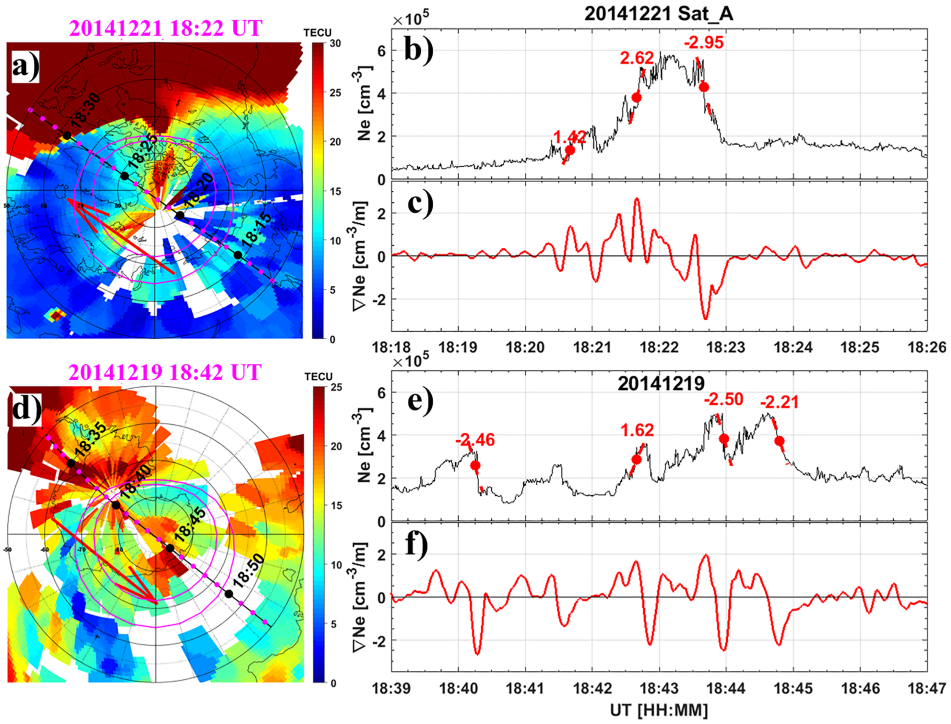

Figure 1. Examples of large-scale density gradients from the Swarm measurements. (a and d) The TEC map showing the ionospheric environment when Swarm A passes the northern and southern polar caps, respectively. The maps are presented in MLAT/MLT coordinates. Black segments present the orbits with timestamps annotated. The Feldstein auroral oval (Q = 3) is shown by magenta curves. (b) The raw electron density (black) during 18:18–18:26 UT. The red dashed lines show the linear regressions in the windows centered by red dots, and the slope of each fit is annotated. (c) Density gradients in the running window during the time of interest. (e and f) An example in the southern hemisphere in the same format as (b) and (c).

3. UT and Seasonal Variations

In order to investigate electron density gradients in the polar caps, we first convert the Swarm data into the magnetic Apex coordinates (Richmond, 1995). We use the Swarm data poleward of ±75° MLAT in both hemispheres to construct the statistics. This latitude is chosen for consistency with previous published results (e.g., Coley & Heelis, 1998). The data are divided into 1 hr in UT and five days in day of year. Figure 2a shows the electron density in the northern polar cap. The data are organized such that the *y* axis starts from local summer toward local winter and back to local summer again. To assist the analysis, we also mark the winter solstice and equinoxes as horizontal lines in each panel. It is clear that the averaged density is higher between local summer and equinoxes. There is no clear UT variation in the summertime electron density, while the wintertime electron density shows a clear UT variation, where the density is highest during 18–21 UT and lowest during 6–9 UT. We also plot the solar zenith angle above the north geomagnetic pole in contours. The electron density generally follows the contours of solar zenith angle, where the high densities correspond to low solar zenith angle. This indicates that the solar EUV ionization is the main source of the high-latitude ionosphere.

Figure 2b presents the averaged electron density in the southern polar cap, which shows obvious variation with respect to season and UT. The electron density is lowest during winter solstice. Furthermore, the UT variation is clear during all seasons, where the density peaks around 5–9 UT. This can be explained by the large displacement between the geomagnetic and geographic poles in the southern hemisphere (for more details, see section 4). The large displacement can cause strong diurnal variation of solar zenith angles in the southern polar cap since the polar cap is defined in magnetic coordinates and the solar zenith angle is dependent on geographic coordinates. This effect is clearly illustrated by the solar zenith angle above the south geomagnetic pole as shown by the contours in Figure 2b; that is, during local summer, the solar zenith angle is about 50° near 3 UT versus about 70° around 15 UT. The difference of solar zenith angles between

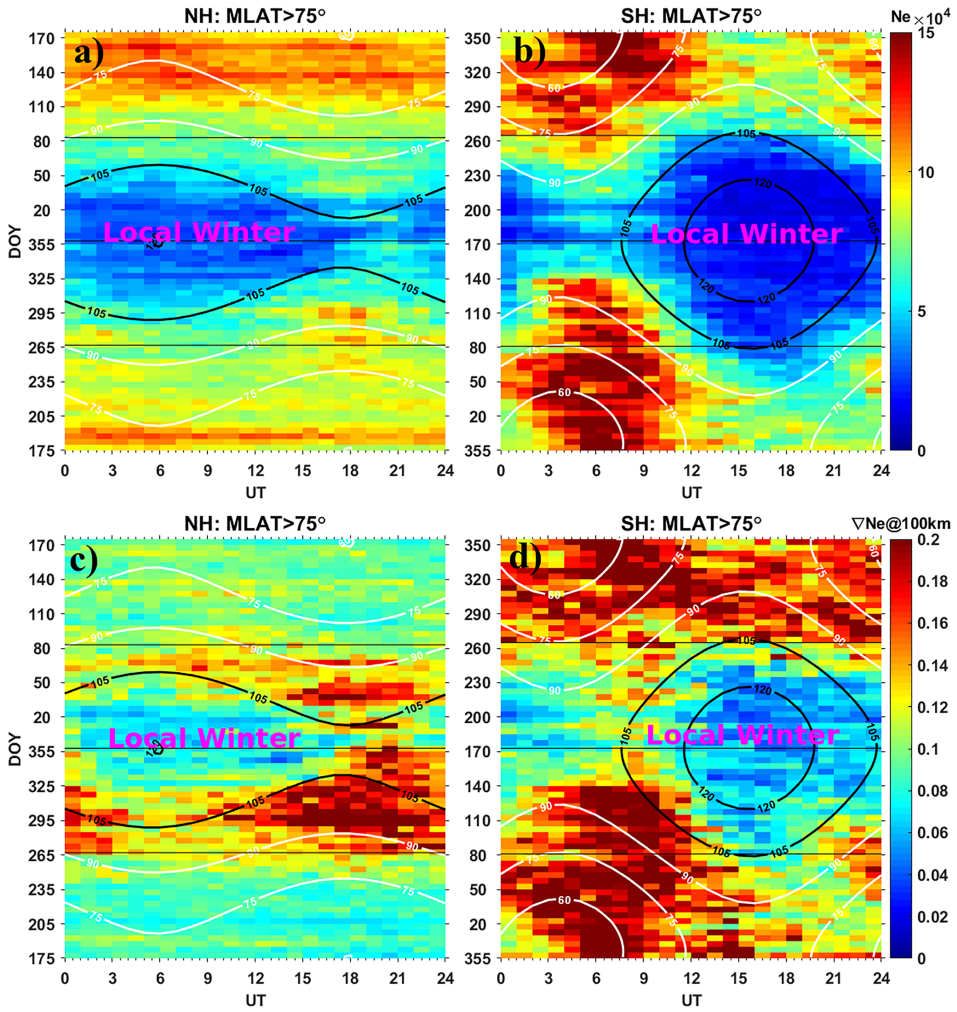

Figure 2. The averaged electron density and averaged density gradient over the spatial scale of 100 km in the polar cap ionosphere (poleward of ±75° MLAT) binned by 1 hr in UT and five days in day of year. (a and b) The averaged electron density in the northern and southern polar caps, respectively. (c and d) The averaged density gradient. In each panel, the solar zenith angle near the altitude of Swarm A above geomagnetic poles in the northern and southern hemispheres are shown in contours. The horizontal black lines show solstices and equinoxes.

summer and winter is very significant, that is, about 50° in summer near 3 UT versus about 130° in winter around 15 UT. This can cause a strong contrast in the ionospheric density between summer and winter and between different UTs due to photoionization. Note that the density during local summer (December) in the Antarctic is higher than that in the Arctic summer (June). This can be attributed to the low solar zenith angle in the Antarctic summer. Additionally, the global ionospheric density is higher during December solstice than during June solstice due to the changing Sun-Earth distance and the neutral composition of the thermosphere (Qian et al., 2013; Rishbeth & Müller-Wodarg, 2006).

With the Swarm data set, we present the climatological features of large-scale density gradients with respect to season and UT for the first time. Figures 2c and 2d show the density gradient in the northern and southern polar caps, respectively. To construct the statistics, we firstly derive density gradients from the raw electron density data, as exemplified in Figure 1. The density gradients are rectified to their absolute values. The absolute values are then binned by 1 hr in UT and five days in day of year. The strong density gradient in the Arctic is confined to days from spring to autumn with an obvious "hole" near December solstice during 3–15 UT. The distribution of the averaged density gradient in the Arctic is similar to the patch to background ratio in the numerical simulation by Sojka et al. (1994). The similarity confirms the validity of using large-scale density gradients as an indication of the high-latitude ionospheric structures.

The distribution of density gradients in the Antarctic behaves quite differently from the northern one as displayed in Figure 2d. However, if we only concentrate on the distribution during days 80–275 (i.e., near local winter), we find that the distribution is similar to the Arctic one during local winter (mirror symmetry) except that the peak density gradient is shifted by ~12 hr in UT. That is, the peak density gradient in the Antarctic is around 7 UT in contrast to 19 UT in the Arctic. This indicates that the production mechanisms, which create density gradients and plasma structures, should be similar during local winter in both polar caps. However, when focusing on the summertime, density gradients become very high and persistent during all UTs. This feature is on the contrary to Figure 2c near the Arctic summer. This is the "real" interhemispheric asymmetry of the electron density gradients.

4. The Spatial Distribution of Density Gradients

The interhemispheric asymmetry is often explained by the different offsets between the geographic and geomagnetic poles in the northern and southern hemispheres. In this section, we try to understand the UT and seasonal variations by the displacements and their relation with respect to the solar terminator. Figure 3 shows the spatial distribution of the electron density and density gradient during two seasons (local summer and winter) and around two UTs (7 UT and 19 UT). Considering that Swarm spends ~131 days to cover the measurements over all MLT sectors, we use the Swarm data during 131 days around June and December solstices in each year, respectively, to construct the spatial maps in Figure 3.

In Figure 3, we show the spatial distribution over a large area (poleward of 51° MLAT). This is because horizontal transportation is an important process to redistribute the ionospheric plasma at high latitudes (Carlson, 2012; Lockwood & Carlson, 1992). The plasma condition over a large area can help to better understand the global distribution of the ionospheric density and gradient.

Near June solstice (Figures 3a–3d), the whole Arctic polar cap is illuminated by sunlight (see the solar terminator in Figures 3a–3d). As a result, the ionospheric density is high due to photoionization. The density in the polar cap is similar around the two UTs (7 UT and 19 UT). Although the density is high during summer, Figures 3c and 3d show that the density gradients are relatively small for both UTs.

Around 7 UT in winter, the solar terminator (63° MLAT) is too far from the cusp. It is therefore difficult for the convection to intake the high-density plasma from the dayside sunlit ionosphere. Only significantly expanded ionospheric convection could "catch" the high-density plasma and transport them into the polar cap. As shown in Figure 3e, the background electron density in the polar cap is very low and the density is high only near the cusp. These density enhancements could also be caused by soft particle precipitation in the cusp region, which are usually lower in density than those transported from the dayside sunlit area (Goodwin et al., 2015). The density gradient is also very weak and it is mostly located near the cusp area. Around 19 UT, the solar terminator is very close to the cusp. It is much easier to bring the solar EUV ionized plasma from the dayside sunlit ionosphere to the polar cap by the dayside reconnection process. Figure 3f shows that the whole polar cap is populated by relative high densities, which are associated with significant density gradients (Figure 3h). This is the typical feature of polar cap patches that are enhanced density with significant density gradients and irregularities.

With the same assumption, we present the spatial distribution of the electron density and density gradient in the Antarctic in Figure 4. In the southern hemisphere, the displacement between geographic and geomagnetic poles is 14° (comparing to 7° in the northern hemisphere). Therefore, the diurnal variation of the solar zenith angle in the polar cap is very significant (Laundal et al., 2016).

Figures 4a–4d show observations during local winter (around June solstice). Around 7 UT, the solar terminator is close to the dayside cusp. As a result, the convection can easily take the high-density plasma from the dayside sunlit ionosphere into the polar cap. We observe high-density plasma in the polar cap (Figure 4a). Figure 4c shows very strong density gradients in the polar cap. However, around 19 UT, the solar terminator is too far equatorward from the dayside cusp, where the solar terminator is located at ~−51° MLAT around MLT noon. The high-latitude convection under normal conditions is not able to transport the plasma from the dayside sunlit ionosphere. This results in very low density in the polar cap as shown in Figure 4b. Figure 4d shows very low values in the density gradient as well.

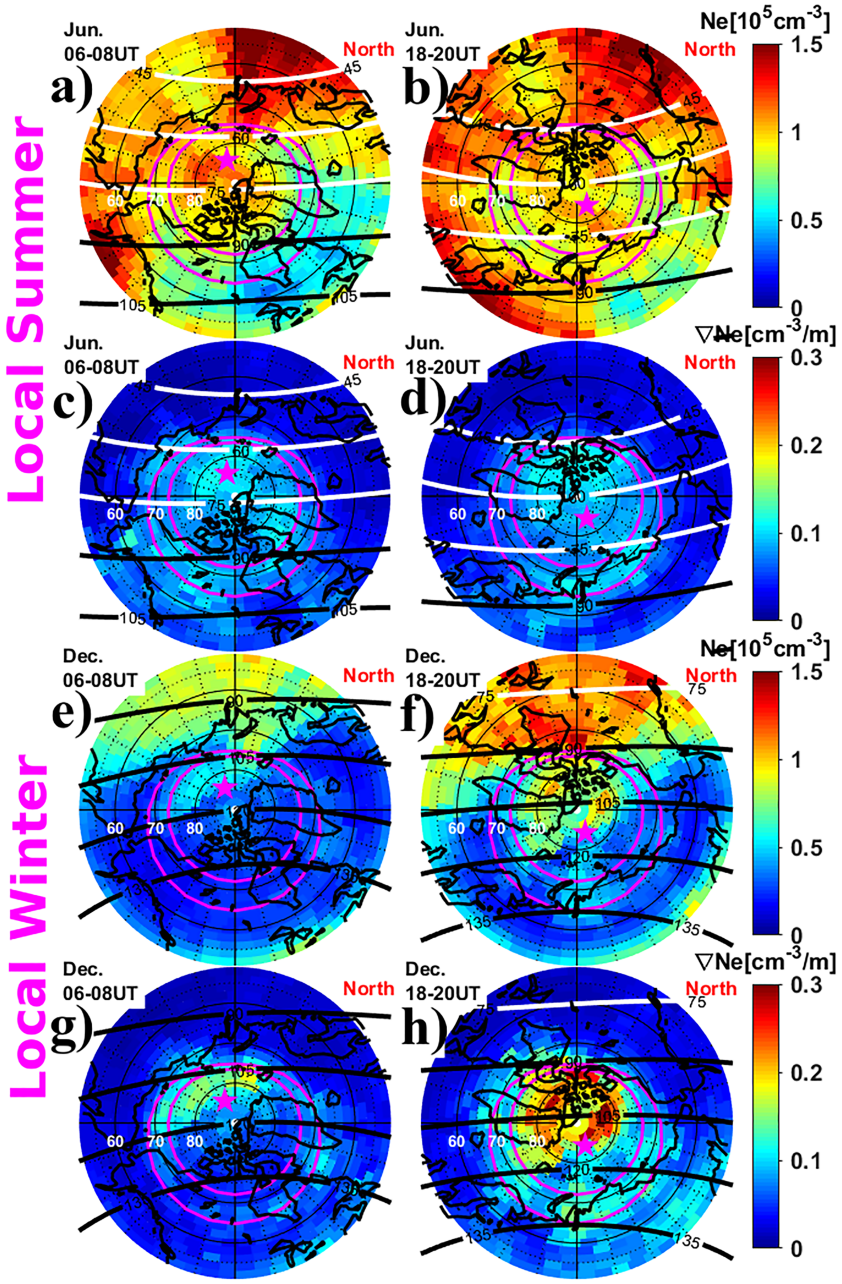

Figure 3. The spatial distribution of the averaged electron density and density gradient around June and December solstices near two UTs. (a and b) The averaged density around the June solstice during 6:00–7:59 UT and 18:00–19:59 UT, respectively. (c and d) The same as (a) and (b) except that they are for the averaged density gradient. (e–h) Similar to (a)–(d) except that they are obtained around the December solstice. In each panel, the spatial distribution is present in MLAT/MLT coordinates. The coastline and solar terminator are overlaid at the middle of the UT intervals (i.e., 7 and 19 UT). The northern geographic pole is shown by a magenta star. The Feldstein auroral oval is presented by magenta curves.

By comparing Figures 3e–3h and 4a–4d (both for local winter), we find that the spatial distributions in both hemispheres are similar. When the solar terminator is close to the cusp, the high-latitude convection has a larger chance of transporting high-density plasma from the sunlit ionosphere into the polar cap. As a result, strong density gradients are observed in the polar cap in this scenario. However, when the solar terminator is too equatorward of the cusp (19 UT in the Arctic and 07 UT in the Antarctic), it is difficult for the high-latitude convection to catch the high-density plasma from the dayside sunlit ionosphere. Therefore, the density gradients are much weaker during such UTs. It is also noted that the density gradients around 7 UT in

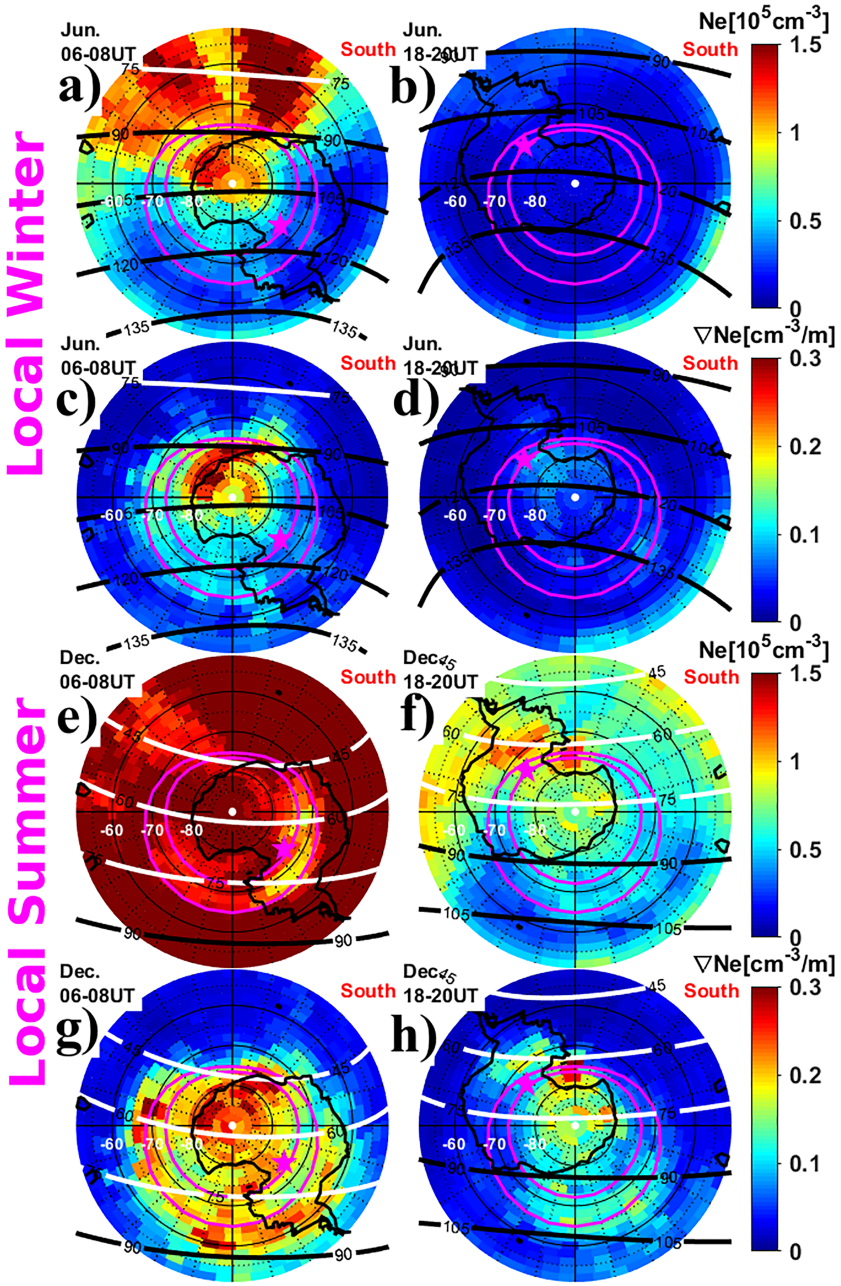

Figure 4. The same as Figure 3 but for the southern hemisphere.

the Antarctic winter are comparable to the gradients at 19 UT in the Arctic winter. Therefore, we conclude that the density gradient and its UT variation in the Antarctic winter are similar to the scenario in the Arctic winter.

Figures 4e–4h show the scenario for local summer in the southern hemisphere. Around 7 UT, the whole polar cap is insolated by sunlight with very low solar zenith angle. Due to the solar EUV ionization, the whole polar cap is filled with high densities. The density gradient is high not only in the polar cap but also near the auroral oval. Around 19 UT, most of the polar cap is illuminated by sunlight even though the solar zenith angle is higher than that around 7 UT. Due to the high solar zenith angle, the density at 19 UT is significantly lower than that at 7 UT. Strong density gradients can be found in the polar cap and near the auroral oval; however, they are weaker than those at 7 UT.

By comparing Figures 3a–3b and 4e–4g (both for local summer), we see a clear difference in the spatial distributions of density gradients. The mystery of the interhemispheric asymmetry is the production and maintenance of density gradients in the Antarctic summer (December).

5. Discussion and Summary

We have presented the UT and seasonal variations of the electron density and density gradient in the northern and southern polar caps (poleward of ±75° MLAT). Due to the solar EUV ionization, the electron density in both polar caps is high during equinoxes and local summer and low during local winter. The electron density is dependent on UT; that is, the electron density in the Arctic is highest around 19 UT, and it is highest around 7 UT in the Antarctic. The UT variations are more prominent in the southern hemisphere. The UT dependence is explained by the displacements from the geographic to the geomagnetic poles, and the larger displacement (14°) explains stronger UT variations in the Antarctic (cf. Figures 3 and 4).

The UT variations and spatial distributions of density gradients in the Arctic and Antarctic are similar during local winter except that they are reversed by 12 hr. Therefore, it is a mirror symmetry between two hemispheres during local winter (December in the Arctic and June in the Antarctic). The UT variations of density gradients are also explained by the impact of the displacements. The cusp is the key region for the high-density plasma to enter the polar cap. When the solar terminator is close to the cusp, the high-density plasma from the sunlit ionosphere can enter the dark polar cap where the background density is very low. In this way, very strong density gradients can be formed in the polar cap.

The density gradients in both hemispheres are strong and persistent during local winter. This is similar to the distribution of polar cap patches from numerical simulations (Sojka et al., 1994), ground-based GPS TEC map (David et al., 2016), and satellite-based observations (Chartier et al., 2018; Noja et al., 2013; Spicher et al., 2017). This type of variation is further verified by ground-based GPS scintillation studies (Jin et al., 2018). This feature has been explained by the variation of the thermospheric neutral composition (e.g., O/N_2; Wood & Pryse, 2010). The density drawn from the dayside ionosphere has a much shorter lifetime during summer than during winter (Schunk & Sojka, 1987). Furthermore, the maintenance of the background density by photoionization in the summertime polar cap smoothes out the large-scale structures that are transported from the dayside lower latitude region (Spicher et al., 2017). Altogether, the plasma structures and density gradients are much lower in the Arctic summer.

So far, the only unexplained feature is strong density gradients in the Antarctic summer. This is the true nature of the north-south asymmetry in density gradients and plasma structures. Due to the sparsity of instruments, very few studies have been conducted in the Antarctic to address the summertime plasma structures, and contradictory results remain (Chartier et al., 2018; Chartier et al., 2019; David et al., 2019; Li et al., 2010; Liu et al., 2017; Noja et al., 2013; Spicher et al., 2017). In this study, we sharpen this question and propose the following mechanism.

The ionospheric density gradient is controlled by two factors, that is, creation and damping. The persistence of density gradients in the Antarctic summer can be due to strong creation and/or slow damping process. The creation term includes the high-latitude convection and flow channels that can mix ionospheric densities of different origin (note that here the creation process is different from the production of ionosphere due to ionization because we focus on density gradients instead of density). Particle precipitation (especially the cusp-type soft precipitation) is another production mechanism that can modulate the ionospheric density and create large-scale density gradients (Jin et al., 2015; Moen et al., 2012). We have checked the spatial distribution of the electron density during local summer (December). The low solar zenith angle suggests a high background density due to photoionization. As suggested by Rodger and Graham (1996), the auroral dynamics can easily create ionospheric structures and produce density gradients on the top of high-density plasma. It is noted that the large-scale field-aligned current is stronger during local summer than during local winter due to higher ionospheric conductivity (e.g., Coxon et al., 2016). The field-aligned currents are closely linked to flow channels and particle precipitation in the high-latitude ionosphere. Therefore, we expect that more density gradients can be created during summer as compared to winter because more energy and momentum are deposited into the high-latitude ionosphere from the solar wind and magnetosphere. The damping of large-scale structures (>100 km) is mainly due to the chemical recombination (Tsunoda, 1988). The chemical recombination can be affected by the thermospheric composition change

or due to the upward plasma drift of the ionosphere. The upward drift can be due to upward $\mathbf{E} \times \mathbf{B}$ drift (due to nonvertical magnetic field) or neutral winds (Liu et al., 2016). In the literature there are studies on the north-south asymmetry of the neutral wind and ion drift and their seasonal and solar activity dependencies (e.g., Cnossen & Förster, 2016; Foerster & Cnossen, 2013). However, the relative contributions of these factors for the persistent density gradients in the Antarctic summer should be carefully examined in future studies.

We have presented the first long-term statistics of electron density gradients in the northern and southern polar caps that focus on UT and seasonal variations. The UT variations and spatial distributions are (mirror) symmetric during local winter (December in the Arctic and June in the Antarctic) between hemispheres. The true asymmetry (anomaly) occurs during December solstice in the Antarctic. In the present study, we focus on the large-scale (100 km) density gradients that are mainly caused by polar cap patches. However, due to the cascading of plasma irregularities from large to small scales, the results are not only confined to large scales. The density gradients presented in this study have implication for ionospheric scintillations (responsive to tens to hundreds of meters) and high-frequency radars (responsive to decameter scales). Further studies are needed to fully understand the creation and maintenance of strong density gradients in the Antarctic summer. For example, such a comparative study can be done by simulations using the Thermosphere-Ionosphere Electrodynamics General Circulation Model.

Acknowledgments
The research is partially supported by the Research Council of Norway under grant 275655. This research is a part of the 4DSpace Strategic Research Initiative at the University of Oslo. The GPS TEC data for GPS TEC map in Figure 1 can be obtained through the Madrigal database (http://cedar.openmadrigal.org), and we acknowledge Dr. Anthea Coster for making TEC data available. The Swarm data can be obtained through the official Swarm website ftp://Swarm-diss.eo.esa.int.

References

Anderson, D. N., Buchau, J., & Heelis, R. A. (1988). Origin of density enhancements in the winter polar-cap ionosphere. *Radio Science*, *23*(4), 513–519. https://doi.org/10.1029/RS023i004p00513

Basu, S., Basu, S., Costa, E., Bryant, C., Valladares, C. E., & Livingston, R. C. (1991). Interplanetary magnetic-field control of drifts and anisotropy of high-latitude irregularities. *Radio Science*, *26*(4), 1079–1103. https://doi.org/10.1029/91rs00586

Buchau, J., Reinisch, B. W., Anderson, D. N., Weber, E. J., & Dozois, C. (1988). Polar-cap plasma convection measurements and their relevance to the modeling of the high-latitude ionosphere. *Radio Science*, *23*(4), 521–536. https://doi.org/10.1029/RS023i004p00521

Buchau, J., Weber, E. J., Anderson, D. N., Carlson, H. C., Moore, J. G., Reinisch, B. W., & Livingston, R. C. (1985). Ionospheric structures in the polar-cap: Their origin and relation to 250-MHz scintillation. *Radio Science*, *20*(3), 325–338. https://doi.org/10.1029/RS020i003p00325

Carlson, H. C. (2012). Sharpening our thinking about polar cap ionospheric patch morphology, research, and mitigation techniques. *Radio Science*, *47*, RS0L21. https://doi.org/10.1029/2011rs004946

Carlson, H. C., Moen, J., Oksavik, K., Nielsen, C. P., McCrea, I. W., Pedersen, T. R., & Gallop, P. (2006). Direct observations of injection events of subauroral plasma into the polar cap. *Geophysical Research Letters*, *33*, L05103. https://doi.org/10.1029/2005gl025230

Chartier, A. T., Huba, J. D., & Mitchell, C. N. (2019). On the annual asymmetry of high-latitude sporadic *F*. *Space Weather-the International Journal of Research and Applications*, *17*, 1618–1626. https://doi.org/10.1029/2019sw002305

Chartier, A. T., Mitchell, C. N., & Miller, E. S. (2018). Annual occurrence rates of ionospheric polar cap patches observed using Swarm. *Journal of Geophysical Research: Space Physics*, *123*(3), 2327–2335. https://doi.org/10.1002/2017ja024811

Cnossen, I., & Förster, M. (2016). North-south asymmetries in the polar thermosphere-ionosphere system: Solar cycle and seasonal influences. *Journal of Geophysical Research: Space Physics*, *121*, 612–627. https://doi.org/10.1002/2015ja021750

Coley, W. R., & Heelis, R. A. (1998). Seasonal and universal time distribution of patches in the northern and southern polar caps. *Journal of Geophysical Research, Space Physics*, *103*(A12), 29,229–29,237. https://doi.org/10.1029/1998ja900005

Coxon, J. C., Milan, S. E., Carter, J. A., Clausen, L. B. N., Anderson, B. J., & Korth, H. (2016). Seasonal and diurnal variations in AMPERE observations of the Birkeland currents compared to modeled results. *Journal of Geophysical Research: Space Physics*, *121*, 4027–4040. https://doi.org/10.1002/2015ja022050

Crowley, G., Ridley, A. J., Deist, D., Wing, S., Knipp, D. J., Emery, B. A., et al. (2000). Transformation of high-latitude ionospheric *F* region patches into blobs during the March 21, 1990, storm. *Journal of Geophysical Research, Space Physics*, *105*(A3), 5215–5230. https://doi.org/10.1029/1999ja900357

David, M., Sojka, J. J., Schunk, R. W., & Coster, A. J. (2016). Polar cap patches and the tongue of ionization: A survey of GPS TEC maps from 2009 to 2015. *Geophysical Research Letters*, *43*, 2422–2428. https://doi.org/10.1002/2016gl068136

David, M., Sojka, J. J., Schunk, R. W., & Coster, A. J. (2019). Hemispherical shifted symmetry in polar cap patch occurrence: A survey of GPS TEC maps from 2015–2018. *Geophysical Research Letters*, *46*(19), 10,726–10,734. https://doi.org/10.1029/2019gl083952

Emmert, J. T., Richmond, A. D., & Drob, D. P. (2010). A computationally compact representation of Magnetic-Apex and Quasi-Dipole coordinates with smooth base vectors. *Journal of Geophysical Research, Space Physics*, *115*. https://doi.org/10.1029/2010ja015326

Foerster, M., & Cnossen, I. (2013). Upper atmosphere differences between northern and southern high latitudes: The role of magnetic field asymmetry. *Journal of Geophysical Research: Space Physics*, *118*, 5951–5966. https://doi.org/10.1002/jgra.50554

Goodwin, L. V., Iserhienrhien, B., Miles, D. M., Patra, S., van der Meeren, C., Buchert, S. C., et al. (2015). Swarm in situ observations of *F* region polar cap patches created by cusp precipitation. *Geophysical Research Letters*, *42*, 996–1003. https://doi.org/10.1002/2014gl062610

Holzworth, R. H., & Meng, C. I. (1975). Mathematical representation of auroral oval. *Geophysical Research Letters*, *2*(9), 377–380. https://doi.org/10.1029/GL002i009p00377

Hosokawa, K., Kashimoto, T., Suzuki, S., Shiokawa, K., Otsuka, Y., & Ogawa, T. (2009). Motion of polar cap patches: A statistical study with all-sky airglow imager at Resolute Bay, Canada. *Journal of Geophysical Research, Space Physics*, *114*, A04318. https://doi.org/10.1029/2008ja014020

Jin, Y., Spicher, A., Xiong, C., Clausen, L. B. N., Kervalishvili, G., Stolle, C., & Miloch, W. J. (2019). Ionospheric plasma irregularities characterized by the Swarm satellites: Statistics at high latitudes. *Journal of Geophysical Research: Space Physics*, *0*(0). https://doi.org/10.1029/2018JA026063

Jin, Y. Q., Miloch, W. J., Moen, J. I., & Clausen, L. B. N. (2018). Solar cycle and seasonal variations of the GPS phase scintillation at high latitudes. *Journal of Space Weather and Space Climate*, *8*. https://doi.org/10.1051/swsc/2018034

Jin, Y. Q., Moen, J. I., & Miloch, W. J. (2014). GPS scintillation effects associated with polar cap patches and substorm auroral activity: direct comparison. *Journal of Space Weather and Space Climate*, *4*. https://doi.org/10.1051/swsc/2014019

Jin, Y. Q., Moen, J. I., & Miloch, W. J. (2015). On the collocation of the cusp aurora and the GPS phase scintillation: A statistical study. *Journal of Geophysical Research: Space Physics*, *120*, 9176–9191. https://doi.org/10.1002/2015ja021449

Kintner, P. M., Ledvina, B. M., & De Paula, E. R. (2007). GPS and ionospheric scintillations. *Space Weather-the International Journal of Research and Applications*, *5*. https://doi.org/10.1029/2006sw000260

Knudsen, D. J., Burchill, J. K., Buchert, S. C., Eriksson, A. I., Gill, R., Wahlund, J. E., et al. (2017). Thermal ion imagers and Langmuir probes in the Swarm electric field instruments. *Journal of Geophysical Research: Space Physics*, *122*, 2655–2673. https://doi.org/10.1002/2016ja022571

Laundal, K. M., Cnossen, I., Milan, S. E., Haaland, S. E., Coxon, J., Pedatella, N. M., et al. (2017). North-south asymmetries in Earth's magnetic field. *Space Science Reviews*, *206*(1-4), 225–257. https://doi.org/10.1007/s11214-016-0273-0

Laundal, K. M., Gjerloev, J. W., Ostgaard, N., Reistad, J. P., Haaland, S., Snekvik, K., et al. (2016). The impact of sunlight on high-latitude equivalent currents. *Journal of Geophysical Research: Space Physics*, *121*, 2715–2726. https://doi.org/10.1002/2015ja022236

Li, G. Z., Ning, B. Q., Ren, Z. P., & Hu, L. H. (2010). Statistics of GPS ionospheric scintillation and irregularities over polar regions at solar minimum. *GPS Solutions*, *14*(4), 331–341. https://doi.org/10.1007/s10291-009-0156-x

Liu, J., Wang, W., Burns, A., Solomon, S. C., Zhang, S., Zhang, Y., & Huang, C. (2016). Relative importance of horizontal and vertical transports to the formation of ionospheric storm-enhanced density and polar tongue of ionization. *Journal of Geophysical Research: Space Physics*, *121*, 8121–8133. https://doi.org/10.1002/2016ja022882

Liu, J., Wang, W. B., Burns, A., Liu, L. B., & McInerney, J. (2017). A TIEGCM numerical study of the source and evolution of ionospheric *F*-region tongues of ionization: Universal time and interplanetary magnetic field dependence. *Journal of Atmospheric and Solar-Terrestrial Physics*, *156*, 87–96. https://doi.org/10.1016/j.jastp.2017.03.005

Lockwood, M., & Carlson, H. C. (1992). Production of polar-cap electron-density patches by transient magnetopause reconnection. *Geophysical Research Letters*, *19*(17), 1731–1734. https://doi.org/10.1029/92gl01993

Lomidze, L., Knudsen, D. J., Burchill, J., Kouznetsov, A., & Buchert, S. C. (2018). Calibration and validation of Swarm plasma densities and electron temperatures using ground-based radars and satellite radio occultation measurements. *Radio Science*, *53*, 15–36. https://doi.org/10.1002/2017rs006415

Lorentzen, D. A., Shumilov, N., & Moen, J. (2004). Drifting airglow patches in relation to tail reconnection. *Geophysical Research Letters*, *31*, L02806. https://doi.org/10.1029/2003gl017785

Moen, J., Gulbrandsen, N., Lorentzen, D. A., & Carlson, H. C. (2007). On the MLT distribution of *F* region polar cap patches at night. *Geophysical Research Letters*, *34*, L14113. https://doi.org/10.1029/2007gl029632

Moen, J., Oksavik, K., Abe, T., Lester, M., Saito, Y., Bekkeng, T. A., & Jacobsen, K. S. (2012). First in-situ measurements of HF radar echoing targets. *Geophysical Research Letters*, *39*, L07104. https://doi.org/10.1029/2012gl051407

Noja, M., Stolle, C., Park, J., & Luhr, H. (2013). Long-term analysis of ionospheric polar patches based on CHAMP TEC data. *Radio Science*, *48*, 289–301. https://doi.org/10.1002/rds.20033

Qian, L., Burns, A. G., Solomon, S. C., & Wang, W. (2013). Annual/semiannual variation of the ionosphere. *Geophysical Research Letters*, *40*, 1928–1933. https://doi.org/10.1002/grl.50448

Richmond, A. D. (1995). Ionospheric electrodynamics using magnetic apex coordinates. *Journal of Geomagnetism and Geoelectricity*, *47*(2), 191–212. https://doi.org/10.5636/jgg.47.191

Rideout, W., & Coster, A. (2006). Automated GPS processing for global total electron content data. *GPS Solutions*, *10*(3), 219–228. https://doi.org/10.1007/s10291-006-0029-5

Rishbeth, H., & Müller-Wodarg, I. C. F. (2006). Why is there more ionosphere in January than in July? The annual asymmetry in the F_2-layer. *Annales Geophysicae*, *24*(12), 3293–3311. https://doi.org/10.5194/angeo-24-3293-2006

Rodger, A. S., & Graham, A. C. (1996). Diurnal and seasonal occurrence of polar patches. *Annales Geophysicae-Atmospheres Hydrospheres and Space Sciences*, *14*(5), 533–537. https://doi.org/10.1007/s00585-996-0533-5

Schunk, R. W., & Sojka, J. J. (1987). A theoretical-study of the lifetime and transport of large ionospheric density structures. *Journal of Geophysical Research, Space Physics*, *92*(A11), 12,343–12,351. https://doi.org/10.1029/JA092iA11p12343

Sojka, J. J., Bowline, M. D., & Schunk, R. W. (1994). Patches in the polar ionosphere: UT and seasonal dependence. *Journal of Geophysical Research, Space Physics*, *99*(A8), 14,959–14,970. https://doi.org/10.1029/93ja03327

Spicher, A., Cameron, T., Grono, E. M., Yakymenko, K. N., Buchert, S. C., Clausen, L. B. N., et al. (2015). Observation of polar cap patches and calculation of gradient drift instability growth times: A Swarm case study. *Geophysical Research Letters*, *42*, 201–206. https://doi.org/10.1002/2014gl062590

Spicher, A., Clausen, L. B. N., Miloch, W. J., Lofstad, V., Jin, Y., & Moen, J. I. (2017). Interhemispheric study of polar cap patch occurrence based on Swarm in situ data. *Journal of Geophysical Research: Space Physics*, *122*, 3837–3851. https://doi.org/10.1002/2016ja023750

Tsunoda, R. T. (1988). High-latitude *F*-region irregularities: A review and synthesis. *Reviews of Geophysics*, *26*(4), 719–760. https://doi.org/10.1029/RG026i004p00719

Weber, E. J., Klobuchar, J. A., Buchau, J., Carlson, H. C., Livingston, R. C., Delabeaujardiere, O., et al. (1986). Polar cap-*F* layer patches: Structure and dynamics. *Journal of Geophysical Research, Space Physics*, *91*(A11), 2121–2129. https://doi.org/10.1029/JA091iA11p12121

Wood, A., & Pryse, S. (2010). Seasonal influence on polar cap patches in the high-latitude nightside ionosphere. *Journal of Geophysical Research Space Physics*, *115*, A07311, https://doi.org/10.1029/2009ja014985